Electronic Research Archive

ERA, 31(5): 2775–2792.
DOI: 10.3934/era.2023140
Received: 04 December 2022
Revised: 15 January 2023
Accepted: 18 January 2023
Published: 13 March 2023

http://www.aimspress.com/journal/ERA

Research article

Optimization of intelligent compaction based on finite element simulation and nonlinear multiple regression

Chengyong Chen[1], Fagang Chang[1], Li Li[2], Wenqiang Dou[1] and Changjing Xu[1,*]

[1] Shandong Hi-Speed infrastructure construction co., LTD, Jinan 250000, China
[2] Shandong Hi-Speed Mansion, Jinan 250000, China

*** Correspondence:** Email: seumayuan@foxmail.com.

Abstract: In intelligent compaction, a critical issue is determining the combination of construction parameters (e.g., the rolling speed and the number of passes) for achieving optimal compaction results. In this paper, a finite element model was developed based on the Mohr-Coulomb elasto-plastic model to simulate the field compaction process of subgrade, which was validated by field compaction tests. Nonlinear multiple regression was used to match the impacts of construction factors on compaction quality based on the model simulation. Then, the linear search approach was used to find the ideal combination of construction parameters that optimizes the compaction quality. The findings indicated that the ideal combination of construction parameters for reaching the ideal compaction degree is a rolling speed of 1.3 m/s with 4 roller passes.

Keywords: intelligent compaction; construction parameters; finite element method; feedback regulation mechanism; optimization

1. Introduction

Compaction is an important part of road construction [1]. Road compaction that meets the target compaction degree can significantly improve its strength [2], stiffness [3], and stability [4], thus ensuring the service life of the road. In the past 50 years, the traditional compaction has made an important contribution to the road infrastructure construction [5]. However, traditional compaction has the following problems [6]: i) the construction parameters of the compaction process, such as the

number of roller passes and the rolling speed, are usually empirically determined according to the operator's experience [7]; ii) the compaction quality detection methods are typically destructive [8], local [9] and non-real-time [10].

The advancement in intelligent compaction (which integrates computer, sensing, and automation technology into compaction technology [11]) has provided the opportunity to solve the drawbacks of traditional road compaction technology and compaction quality control [12]. The remaining problems are mainly related to the complex material behavior during compaction, and the feedback control in intelligent compaction. The complexity of material behavior is primarily due to the large plastic deformation in compaction, which leads to the dramatic change in material properties [13], for example, the change of yield condition with the increase in the material's density. In the literature on intelligent compaction simulation, subgrade parameters are mostly assumed as fixed parameters without considering their changes during compaction [14], which can be a primary source of errors. Research on the intelligent compaction feedback adjustment method is still in its early stages [15]. It is still not clear what is the optimal combination of construction parameters [16]. A reliable mechanism for adjusting the construction parameters in real-time, according to the actual compaction state, is still lacking, which affects the construction quality and efficiency, and causes a waste of resources [17].

Travel parameters, excitation parameters, and material parameters are the three main construction parameters of intelligent compaction. Since the material parameters are relatively consistent for the same site in the compaction process, when the model of the vibratory roller is determined, its excitation parameters usually only have 2 or 3 options with a low range of variation. In contrast, travel parameters are more controllable by roller operators, and thus exhibit a much wider range of variation [18]. In this paper, we focus on the travel parameters of intelligent compaction, which include the rolling speed and the number of roller passes. A finite element model is developed to simulate the effects of these travel parameters on compaction quality. The Mohr-Coulomb elasto-plastic model is used to simulate the compaction behavior of the subgrade material, considering the change of the material parameters with the increase in compaction degree. The model is further validated by the results of field tests. Based on the simulation results, the optimal combination of travel parameters for maximizing the compaction quality is obtained by the linear search method. Based on this, the feedback adjustment method of the input parameters is discussed.

2. Methodology

2.1. Finite element simulation of subgrade compaction

The ABAQUS finite element software is employed for the finite element simulation. The most fundamental and essential part of the finite element model is selecting the material model and determining the model parameters. In this paper, the Mohr-Coulomb elasto-plastic model is used for representing the subgrade material. In the Mohr-Coulomb model, the plastic deformation of the soil is expressed by the shear strength indices (cohesion c, internal friction angle φ). The established model needs to reflect the change of shear strength indices during the compaction of the subgrade. To this end, the real-time compaction degree K is chosen as a "field variable", and its effects on the shear strength indices are considered in this study. The relationship between K and soil shear strength indices are then established through laboratory experiments. In the numerical method, the relationship between K and shear strength indices is captured through a UMAT subroutine of the ABAQUS software. Since the strain of the soil body can be obtained in real-time in the finite element program, the shear strength

indices can be updated in real-time by the above method. More details of this material model are described in Sections 2.1.1 and 2.1.2.

2.1.1. Relationship between *K* and subgrade strain

The simulation model is built with the following assumptions [19]:
1) The dimensions in the horizontal and vertical directions during the compaction of the subgrade is negligible compared to the model dimensions, and the model shape during compaction is considered rectangular.
2) The subgrade soil is continuous, uniform and isotropic in the initial state and during compaction. The width in the z-direction is set to 1 in the model, and no deformation occurs, i.e., strain $\varepsilon_3 = 0$. The initial compaction degree K_0 is set to 0.8. The calculation process and expressions for the volume of the subgrade soil model in the compaction process are shown in Eq (1):

$$\begin{aligned} V_1 &= x\ y\ z\ (1+\varepsilon_1)\ (1+\varepsilon_2)(1+\varepsilon_3) \\ &= x\ y\ z\ (1+\varepsilon_1)\ (1+\varepsilon_2)(1+0) \\ &= x\ y\ z\ (1+\varepsilon_1)\ (1+\varepsilon_2) \\ &= V_0\ (1+\varepsilon_1)\ (1+\varepsilon_2) \end{aligned} \tag{1}$$

where: x - the length of the model (m); y - the thickness of the layer to be compacted by the model (m); z - the width of the model (m), since the model is a two-dimensional model, z = 1 m; ε_1 - strain in x-direction; ε_2 - strain in y-direction; ε_3 - strain in the z-direction, $\varepsilon_3 = 0$; V_0 - the initial volume of the model.

The real-time compaction degree K can be calculated by Eq (2):

$$K = \frac{\rho}{\rho_{max}} \tag{2}$$

The density ρ and the maximum dry density ρmax are calculated according to Eq (3):

$$\rho = \frac{m}{V}, \rho_{\max} = \frac{m}{V_{\min}} \tag{3}$$

where: K -- real-time compaction; ρ -- density under real-time compaction K corresponding to (kg/m^3); ρ_{max} -- maximum dry density (kg/m^3); m --mass (kg) corresponding to density ρ; V --volume (m^3) corresponding to density ρ; V_{min} --volume (m^3) corresponding to maximum dry density ρ_{max}.

During compaction, the soil mass m is a constant value, the maximum dry density ρ_{max} of the soil remains unchanged, the volume V_{min} corresponding to the maximum dry density ρ_{max} remains unchanged, and only the volume V and density ρ change in real-time. Combining Eqs (1)–(3), Eq (4) can be obtained as follows:

$$K = \frac{V_{\min}}{V_0(1+\varepsilon_1)\ (1+\varepsilon_2)} \tag{4}$$

From the initial setting of compaction ρ_1 of 0.8, the final relationship between real-time compaction K and strain can be obtained by substituting Eq (4), as shown in Eq (5):

$$K = \frac{0.8}{(1+\varepsilon_1)\ (1+\varepsilon_2)} \tag{5}$$

So far, the relationship between real-time compaction K and strain ε has been established.

2.1.2. Relationship between K and shear strength indices of subgrade soil

In a previous study by the authors [20], direct shear tests were carried out on yellow-pan chalk soil specimens, cylindrical specimens with compaction degrees of 80, 85, 90, 93, 94, 96 and 100% were prepared for direct shear testing in the laboratory tests. The test results are shown in Table 1.

Table 1. Test results of compaction degree, cohesion, and internal friction Angle.

Compaction Degree/ K	Cohesion/ c(kPa)	Internal Friction Angle/ φ(°)
0.8	12.1	27
0.85	41.2	28.8
0.9	58.6	31.2
0.93	61.6	30.5
0.94	62.8	32.4
0.96	63.6	34.3
1	74.9	36.9

By fitting, the equations for the relationship between real-time compaction degree K and cohesion c and compaction and internal friction angle φ are obtained as:

$$\begin{aligned} c &= -1248K^2 + 2532.8K - 1213.3 \\ \varphi &= 46.7K - 11.1 \end{aligned} \tag{6}$$

These relationships are then used in the finite element model. The initial compaction degree K_0 is 0.8, and the maximum compaction degree Kmax is 1. By Eq (8) and choosing 0.01 as the step size of K, the tabulated relationship between K and the shear strength indices is generated, as shown in Table 2.

The data in Table 2 are added in the Abaqus software to achieve the real-time updating of the shear strength indices of the subgrade material during the compaction simulation, thus improving the accuracy of the numerical simulation.

Table 2. The "field" compaction degree K corresponds to the shear strength of soil.

Compaction Degree / K	Cohesion/ c(kPa)	Internal Friction Angle/ φ(°)	Compaction Degree / K	Cohesion/ c(kPa)	Internal Friction Angle/ φ(°)
0.8	26.4	14.2	0.91	31.5	58.1
0.81	26.9	19.5	0.92	32.0	60.6
0.82	27.3	24.4	0.93	32.5	62.8
0.83	27.8	29.2	0.94	32.9	64.8
0.84	28.3	33.7	0.95	33.4	66.5
0.85	28.7	37.9	0.96	33.9	68.0
0.86	29.2	41.9	0.97	34.3	69.3
0.87	29.7	45.6	0.98	34.8	70.3
0.88	30.1	49.1	0.99	35.3	71.0
0.89	30.6	52.4	1	35.7	71.5
0.9	31.1	55.3			

2.1.3. Subgrade structure and meshing

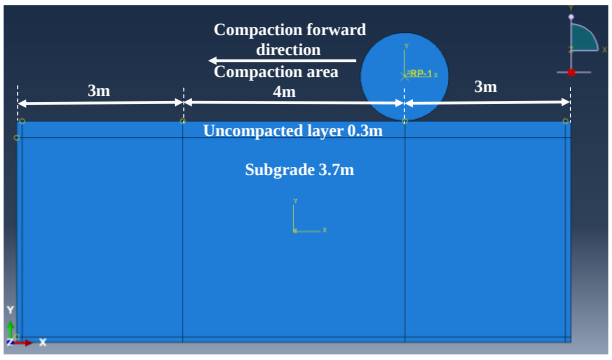

Figure 1. Subgrade structure.

A previous study [21] showed that the influence range of the vibrating wheel in the horizontal direction during compaction is about 3–5 m. Therefore, when establishing the numerical simulation model, the horizontal direction is defined as 10 m, which eliminates the influence of the boundary. In actual construction, each layer of the subgrade is around 20–30 cm in thickness in its loose state. Therefore, in this paper, the loose thickness of the upper layer is defined as 30 cm, and the lower

foundation is defined as 3.7 m thick. The schematic diagram of the subgrade structure is shown in Figure 1. Table 3 gives the parameters of the initial compaction state of the subgrade soil.

Table 3. Parameters of initial compaction state of subgrade soil [20].

Location	Density/ P (kg/m3)	Elasticity Modulus/ E(MPa)	Cohesion/ c(kPa)	Internal Friction Angle/ φ(°)	Poisson's ratio
Upper	1634	15	11.88	27	0.33
Substratum foundation	1859	30	55.8	31.15	0.35

The size of elements is a key to the numerical simulation, which should be selected to ensure both the accuracy and efficiency of the numerical. Related studies have shown [22] that the grid size is related to computational accuracy, and to ensure computational accuracy, the grid size needs to satisfy:

$$\Delta l \le \left(\frac{1}{8} - \frac{1}{10}\right)\lambda \tag{7}$$

where, λ -- the highest frequency corresponding to the wavelength.

The excitation frequency of vibratory rollers is around 25–40 Hz. from Table 3 in the subgrade soil parameters calculated according to Eq (8) to obtain the subgrade soil shear modulus:

$$G = \frac{E}{2(1+\mu)} \tag{8}$$

where, G -- shear modulus (MPa); E -- elastic modulus (MPa); μ – Poisson's ratio. The shear modulus of the subgrade soil is calculated to be 5.64 MPa.

The initial density of the subgrade soil can be calculated according to Eq (9):

$$\rho_0 = \rho_{\max} \cdot K_0 \tag{9}$$

where, ρ_0 -- initial density (kg/m^3). The initial density of the subgrade soil is calculated to be 1472 kg/m^3.

The vibration wave velocity during vibratory compaction of the subgrade soil can be calculated according to Eq (10) [23]:

$$c_s = \sqrt{\frac{G}{\rho}} \tag{10}$$

where, c_s -- vibration wave velocity (m/s). The vibration wave speed during the vibration compaction of the subgrade soil is calculated to be 61.9 m/s.

The wavelength corresponding to the highest frequency (40 Hz) can be calculated according to Eq (11), which yields:

$$\lambda = \frac{c_S}{f} \tag{11}$$

where, f -- the highest frequency (Hz). The wavelength of the vibration wave during the vibration compaction is calculated to be λ = 1.55 m.

The mesh size for the finite element numerical simulation is thus determined as follows:

$$\Delta l \leq (0.16 \sim 0.19)m$$

In this paper, considering the calculation efficiency and accuracy, the grid size is 0.05 m in the center area of the load application and 0.2 m at the boundary. The fine grids are connected with the coarse grids by gradient grids, as shown in Figure 2.

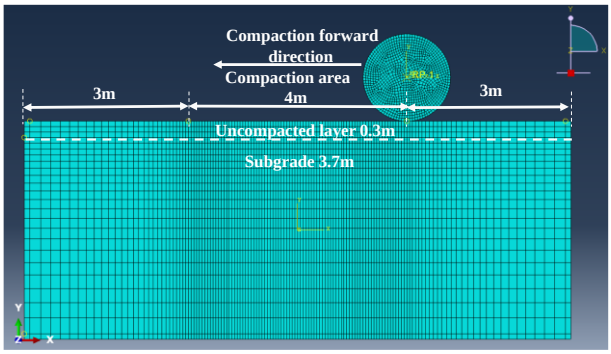

Figure 2. Finite element numerical simulation grid division diagram.

2.1.4. Boundary and loading conditions

The boundary conditions do not significantly affect the simulation results because the model size chosen is sufficiently large. Therefore, the horizontal sides and the ground are set as fixed constraints.

ZhongdaYZ32 machine is a common brand of road roller, so its parameters are chosen as the basic parameters for numerical simulation in this paper. The standard medium and large YZ32 roller were used in this study, whose loading parameters are shown in Table 4. In the simulation, 1–4 roller passes were applied.

Table 4. Numerical simulation input parameter.

Weight of Vibrating Wheel (kg)	Frame Weight (kg)	Excitation Force (kN)	Frequency (Hz)
16,000	16,000	45,000	28

2.2. Travel parameters of the simulation

The travel parameters are the most adjustable and variable in the intelligent compaction process. Therefore, the travel parameters, i.e., the number of passes and the rolling speed, are considered the

main variables in this study. Finite element simulations with different travel parameters are performed to study their effects on the final compaction degree.

In real practice, the rolling speed ranges from 1 to 4 m/s, and the number of roller passes ranges from 2 to 4 passes. Given these ranges, the combinations of travel parameters for the finite element simulations are listed in Table 5.

Table 5. Finite element numerical simulation conditions.

Number	Speed (m/s)	Compaction Pass (time)	Number	Speed (m/s)	Compaction Pass (time)
NO.1	1	2	NO.12	2.5	4
NO.2	1	3	NO.13	3	2
NO.3	1	4	NO.14	3	3
NO.4	1.5	2	NO.15	3	4
NO.5	1.5	3	NO.16	3.5	2
NO.6	1.5	4	NO.17	3.5	3
NO.7	2	2	NO.18	3.5	4
NO.8	2	3	NO.19	4	2
NO.9	2	4	NO.20	4	3
NO.10	2.5	2	NO.21	4	4
NO.11	2.5	3			

By performing the designed 21 simulations, the effects of the travel parameters on the compaction quality can be analyzed, as will be discussed in Section 2.3.

2.3. Field test of subgrade compaction

To verify the accuracy of the numerical simulations, field tests of subgrade compaction were carried out. The site of the field test is the Binzhou section of Zhanlin Expressway in Shandong Province, China. The starting and ending piles of the compaction section are K371 + 000~K371 + 200, a two-way 8-lane expressway, running from north to south. Each lane is divided into two stripes for compaction. Each compaction stripe includes one pre-compaction pass, one leveling pass, four vibration compaction passes, and one static compaction pass. Because the vibratory compaction stage represents the most critical stage of compaction, the numerical simulation and field tests were mainly focused at this stage. The vibratory compaction process is shown in Figure 3.

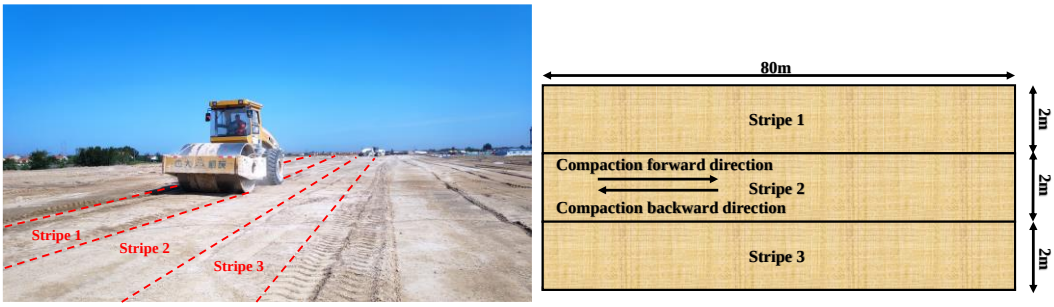

Figure 3. Subgrade vibration compaction field test.

The vibratory roller is Zhongda Machinery YZ32, and the detailed parameters are shown in Table 6.

Table 6. Vibratory roller parameters.

Roller Brand	Frequency (Hz)	Nominal Amplitude (mm)	Exciting Force Amplitude (kN)	Total Weight (t)
YZ32	28/33	1.8/1.1	590/450	32
Front/Rear Wheel Weight(t)	Speed (km/h)	Rated Speed (rad/min)	Roller Width (mm)	Roller Radius (mm)
21/11	0~8	2200	2000	600

In order to ensure the relative accuracy of the test results, the same construction parameters were used in the three compaction stripes, and the degree of dispersion is further compared with the numerical simulation results. The loading parameters of the field test were kept as consistent as possible with the numerical simulation input parameters. The values of the loading parameters are listed in Table 7.

Table 7. Field test parameters.

Roller Weight (kg)	Exciting Force Amplitude (kN)	Frequency (Hz)	Speed (m/s)	Compaction Pass (time)
32,000	45,000	28	2	4

It is seen that the travel parameters of the field test are the same as that of the NO.9 simulation (as shown in Table 5). Therefore, the field test results are compared with the NO.9 simulation to validate the finite element model.

In field tests, the compaction degree was determined by the ring knife method, where densities at three points are measured for each stripe at the end of each roller pass. The average of the three measures was used to represent the compaction degree of the stripe.

2.4. Multiple nonlinear regression analysis

Regression models [24] are used to quantitatively correlate the rolling speed and the number of roller passes with the final compaction degree. A binary nonlinear regression is applied for this purpose [25]. In this study, the binary regression model is assumed to have a binary parabolic function form [26]:

$$K = a_0 + a_1 n + a_2 n^2 + a_3 v + a_4 v^2 \tag{12}$$

where: n -- number of rolling passes (times); v -- rolling speed (m/s); α_i -- coefficient to be determined.

In this paper, the accuracy of the regression is determined by the coefficient of determination r^2 [27], which is defined as:

$$r^2 = 1 - \frac{\sum_i (y_i - \hat{y})^2}{\sum_i (y_i - \bar{y})^2} \tag{13}$$

The closer r^2 is to 1, the higher the predictability of the regression model is. When $r^2 = 1$, it means that the regression model is completely correlated with the real data, that is, a functional relationship; when $r^2 > 0.7$, it means that the regression model has a strong correlation with the real data; when $r^2 = 0$, it means that the regression model has no correlation with the real data [27].

3. Results and discussion

3.1. Numerical simulation results

Through finite element simulation, the variation of vertical displacement corresponding to different construction parameters during road compaction is obtained, and then the trend of compaction degree can be calculated. The relationship between the vertical displacement x and the real-time compaction degree K of the subgrade soil is derived as follows:

Let the initial compaction of the subgrade soil be K_0, the thickness of the subgrade soil loosened is U, and the maximum compaction of the subgrade soil $K_{max} = 1$. In theory, the maximum vertical displacement x_{max} is as follows:

$$x_{\max} = U(1-K_0) \tag{14}$$

The theoretical maximum vertical displacement $x$max corresponds to a compaction growth space of (1–K_0), in which the relationship between the current vertical displacement x, and the compaction can be established as follows:

$$K = K_0 + (1-K_0)\frac{x}{U(1-K_0)} \tag{15}$$

In the research process of this paper, the initial compaction degree $K_0 = 0.8$ is set for the subgrade soil, the thickness U of the top layer of the subgrade is 0.3 m, and the real-time compaction degree and vertical displacement variation can be calculated from Eq (16) as follows.

$$K = 0.8 + 0.2\frac{x}{0.06} \tag{16}$$

where: x -- vertical displacement (m).

The simulation results of the NO.9 parameter set are shown in Figure 4. It is seen from Figure 4(a) that the most significant compaction occurred at the initial roller pass, which causes a vertical displacement of about 3.5 cm (over 70% of the total vertical displacement). The vertical displacement occurs instantaneously when the roller contacts the soil, which, therefore, represents the static compaction due to the self-weight of the roller. During each roller pass, the vertical displacement fluctuates with a small amplitude (around 3 mm) around a stable value. The fluctuation is due to the vibration of the roller. As the number of roller passes increases, the vertical displacement gradually increases, causing the increase in compaction degree as shown in Figure 4(b). It is noticed that the growth rate of the compaction degree becomes slower as the number of roller passes increases, which captures the fact that soil becomes more difficult to compact as the compaction degree increases.

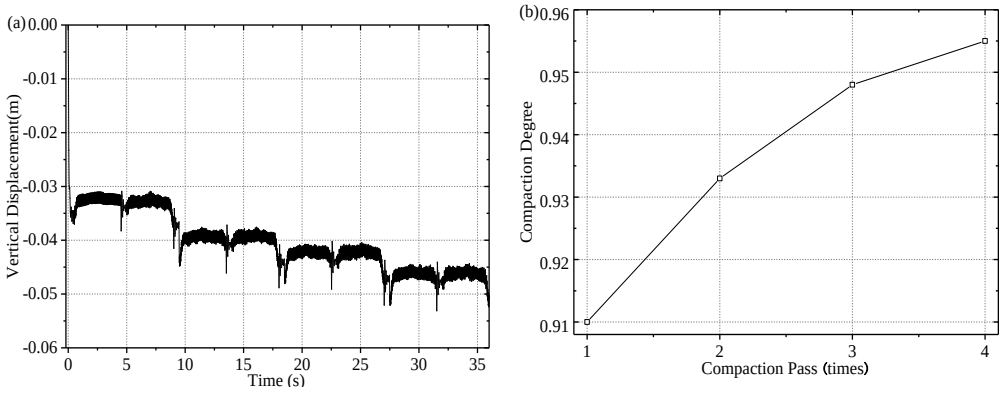

Figure 4. (a) Vertical displacement versus time curve; (b) Trend of compaction degree.

3.2. Comparison between simulation and field tests

In the field compaction tests, the compaction degree was measured by the ring knife method. Three measurements were taken for the three comparison stripes. The average and variability of the compaction degree are shown in Figure 5. As mentioned in the previous section, the NO.9 parameter

set is consistent with the field test conditions. Therefore, the simulation results of the NO.9 parameter set are compared with the field measurements, as shown in Figure 5.

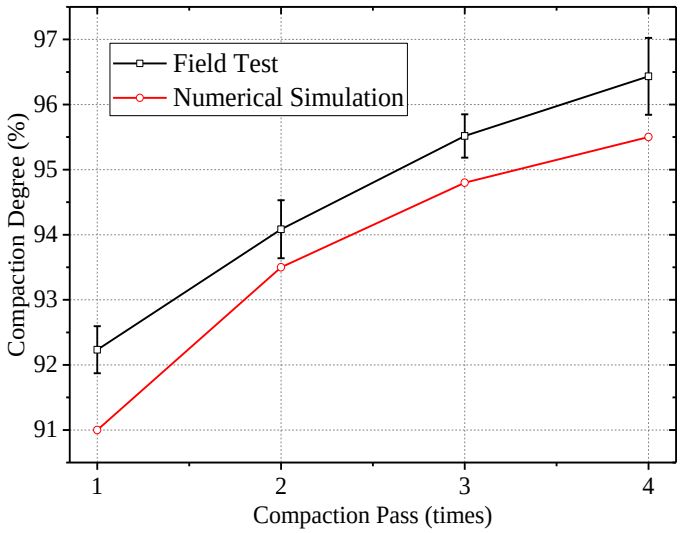

Figure 5. Error bar of compaction variation in field test versus numerical simulation of compaction variation.

Figure 5 shows that the variation of compaction degree shares a similar trend in field tests and simulation. However, the compaction degree of field tests is generally higher than the simulation results by about 1%. This is because, in field compaction, a static compaction and leveling were carried out before the four vibratory compaction, which brought a certain growth in compaction degree of the subgrade. The compaction degree before the vibratory compaction and after leveling is roughly between 80 to 90%, due to the variability of the compaction degree. This is higher than the initial compaction degree used in the finite element numerical simulation $K_0 = 0.8$. It is expected that if a higher K_0 were used in the numerical simulation, the simulation results would match the field results better.

For field tests, the variability in compaction degree was indicated by the error bar in Figure 5. The length of the error bar represents the standard deviation or standard error of the compaction degree. It is seen that the variability in test compaction is relatively small, with standard deviation or standard error of the four roller passes being 0.33, 0.42, 0.32 and 0.57, respectively. The main source of error is the stripe 1, which is located at the outermost boundary and has a smaller compaction degree than stripes 2 and 3. The compaction degree of stripes 2 and 3 are relatively consistent.

3.3. Final compaction degree

By the 21 sets of numerical simulation, the final compaction degrees under different compaction parameters were obtained, as shown in Table 8.

Table 8. The final compaction degree corresponding to each parameter.

Speed (m/s) \ Compaction pass	2	3	4
1	0.933	0.948	0.955
1.5	0.931	0.941	0.949
2	0.939	0.948	0.954
2.5	0.922	0.934	0.944
3	0.904	0.924	0.937
3.5	0.887	0.902	0.918
4	0.878	0.896	0.903

The relationships of compaction degree with the number of roller passes and compaction speed are shown in Figure 6.

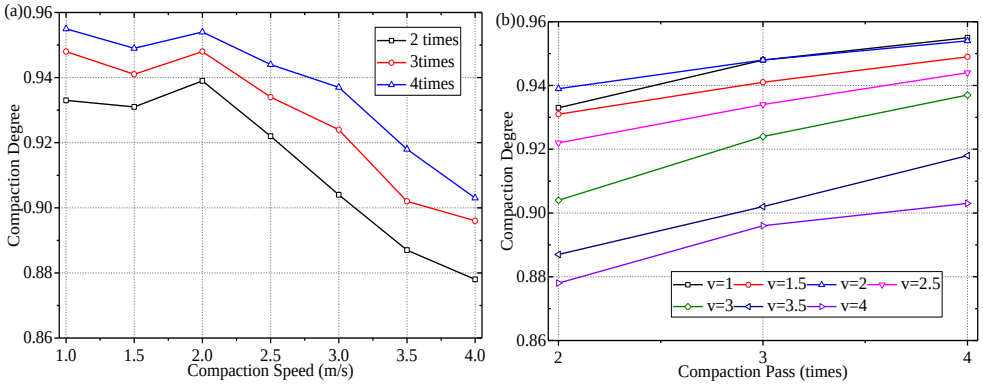

Figure 6. (a) The curve between speed and compaction degree; (b) The curve between compaction passes and compaction degree.

Figure 6(a) shows that the final compaction degree is gradually decreasing with the increase of the rolling speed. This is because that with the increase in rolling speed the time of compaction for a local part by the vibratory roller decreases, which reduces compaction effort of each roller pass. It is noticed that, when the rolling speed is in the range of 1–2 m/s, the final compaction degree is relatively stable. This is because the work done by the vibratory roller on the subgrade at a speed of 2 m/s is close to the upper limit of energy that the subgrade can withstand. Even if the speed is reduced, it is difficult to further compact the subgrade under the condition of other compaction parameters (e.g., excitation force, excitation frequency) as they remain unchanged.

Figure 6(b) shows that as the number of passes increases, the final compaction degree increases, but the growth of compaction decreases gradually. This is because the subgrade become more difficult to compact with the increase in the compaction degree.

After analyzing the single effect of compaction speed or number of roller passes, the coupled effect of two factors on the compaction degree is characterized through a multiple nonlinear regression model, as shown in Eq (17):

$$K = 0.88 + 1.7\times10^{-2}v - 7.2\times10^{-3}v^2 + 2.56\times10^{-2}n - 2.3\times10^{-3}n^2 \tag{17}$$

The coefficient of determination was calculated to be $r^2 = 0.93$, according to Eq (15). Since $r^2 > 0.7$, it indicates that the regression model achieves a sufficient accuracy. Therefore, it can be used to further analyze the optimal combination of marching parameters.

3.4. Optimization of travel parameters for intelligent compaction

Through Eq (17), the optimal combination of travel parameters can be further solved. The interpolation interval of rolling speed is [1,4] with interpolation step of 0.1 m/s, and the interpolation interval of rolling passes is [2,4] with interpolation step of 1 m. The resultant compaction degree corresponding to different rolling speed and number of passes is shown in Figure 7.

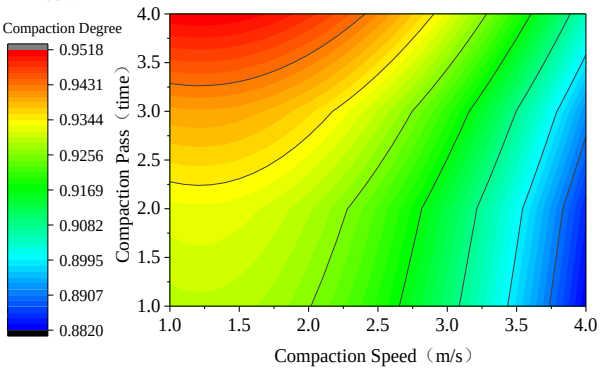

Figure 7. Contour plot of final compaction degree.

Figure 7 shows that, when the rolling speed is 1–1.7 m/s, the number of rolling passes becomes the main control factor affecting the final compaction degree of the subgrade. Within this range of rolling speed, the variation in rolling speed does not have a significant impact on the final compaction degree. This indicates that the rolling speed 1.7 m/s probably represents a the upper limit of the energy input that the soil can absorb in each roller pass. Thus, decreasing rolling speed to lower than 1.7 m/s would not further increase the rate of compaction.

By contrast, when the speed of rolling is 1.7–4 m/s, both the number of passes and the rolling speed have significant effects on compaction. When rolling speed is > 1.7 m/s, the work done by the subgrade on the roller cannot be completely absorbed, so the increase in the rolling speed would decreases the compaction energy, and decreases the final compaction degree.

An optimization is carried out by the linear search method to maximize the final compaction degree. The optimal control parameters are: the optimal rolling speed = 1.3 m/s, and the optimal

number of rolling passes = 4 times. It is seen in Figure 7, at this point, the final compaction degree reaches the maximum.

3.5. Discussion on intelligent compaction feedback adjustment mechanism

The feedback adjustment mechanism is the core research area of intelligent compaction. Its goal is to improve the efficiency of intelligent compaction and guarantee construction quality. The feedback adjustment mechanism can be divided into two parts: the determination of the optimal parameters, and the real-time adjustment of parameters when the current compaction quality does not match the expected compaction quality. This paper focuses on the first part of the feedback adjustment mechanism.

The optimal parameters of the intelligent compaction have been obtained in Section 3.4 based on numerical simulation, which can provide the initial setting for the intelligent compaction feedback adjustment mechanism. The subsequent feedback adjustment part can be carried out on this basis.

3.5.1. Optimal combination of travel parameters and optimal construction efficiency

In practical projects, construction efficiency is usually one of the important factors. In the actual construction process, often the target compaction requirements of the subgrade do not need to reach the maximum. For example, in the construction of the subgrade, the target compaction degree is 95%, while the maximum compaction degree obtained through theoretical calculations is 97%. A variety of parameter combinations can achieve the corresponding 95% compaction degree. Under such circumstance, the construction efficiency must be considered, which can be defined as the total time of the compaction process, Eq (18) is used as a method for construction efficiency evaluation:

$$T = \frac{x}{v} \cdot n = x \cdot \frac{n}{v} \tag{18}$$

where x = Stripe length, v = speed of compaction, and n = compaction pass. The optimum combination of number of passes and speed is determined by minimizing the total construction time T.

3.5.2. Feedback adjustment mechanism

When the current compaction quality does not match the expected compaction quality, the feedback adjustment mechanism is needed to control the compaction quality and efficiency in real time.

A feedback adjustment mechanism based on the idea of extreme difference is proposed in this study, but of course, if the amount of data is large enough, the feedback adjustment mechanism can also be calculated by machine learning or deep learning methods. The proposed adjustment mechanism can be demonstrated through an example of field compaction. The target compaction degree at the second and third roller passes are 0.927 and 0.941 respectively. However, during the compaction, the measured the compaction degree is 0.925, which is lower than the target (0.927), and thus can be referred to as “under-compaction”. Given the detected under-compaction at the second roller pass, adjustment must be made to ensure achieving the target compaction degree at the third roller pass.

The difference between the actual and the target compaction degree after the second roller pass is △K = 0.925-0.927 = -0.002. Substituting △K = -0.002 and n = 3 into Eq (17), the rolling speed v can be obtained by solving the following equation:

$$K = 0.878 + 1.7\times10^{-2}v - 7.2\times10^{-3}v^2 + 2.56\times10^{-2}\times3 - 2.3\times10^{-3}\times3^2 \tag{19}$$

The process of calculating the rolling speed v can also be shown graphically in Figure 8.

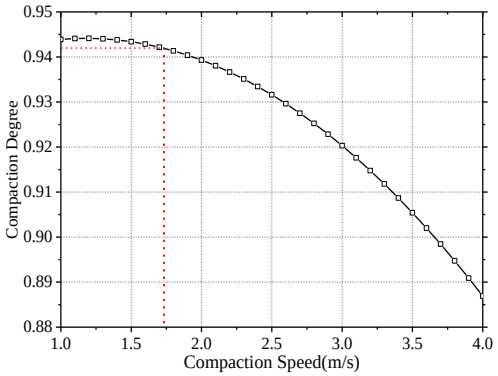

Figure 8. Relation curve of compaction degree versus rolling speed.

It can be seen from Figure 8 that by adjusting the rolling speed from 2 to 1.74 m/s, the target compaction degree of 0.941 can be achieved after the completion of the third rolling, i.e., the target compaction degree requirement is satisfied.

4. Conclusions

In this paper, through the finite element simulation and nonlinear regression of the simulation results, the optimal combination of travel parameters of intelligent compaction of the subgrade is obtained. The conclusions obtained in this paper are as follows:

1) Compaction happens instantaneously as the roller wheel and soil make contact. The initial roller pass has the most significant compaction effect (over 70% of the total compaction). The compaction effect decreases as the increase in the number of roller passes. The compaction degree fluctuates due to the roller vibration, but the amplitude of the fluctuation is generally small compared to the static compaction.

2) The final compaction degree gradually decreases with the increase of the rolling speed. However, when the rolling speed is in the range of 1–1.7 m/s, the final compaction degree does not change significantly.

3) In this paper, the optimal combination of rolling speed and number of rolling passes for the compaction of subgrade soil are 1.3 m/s and 4 times, respectively.

In this paper, a specific soil type, the yellow-pan chalk, was studied. Future studies are suggested to cover a wider range of soil types. The optimal combination of travel parameters should also be calculated for different soil types to extend the applicability of the approach proposed in this study.

Acknowledgments

This paper was supported by Department of Transportation of Shandong Province (No. 2018B51).

Conflict of interest

We declare that there are no conflicts of interest.

References

1. P. Vennapusa, D. White, S. Schram, Roller-integrated compaction monitoring for hot-mix asphalt overlay construction, *J. Transp. Eng.*, **139** (2013), 1164–1173. https://doi.org/10.1061/(ASCE)TE.1943-5436.0000602
2. T. Chen, T. Ma, X. Huang, S. Ma, S. Wu, Microstructure of synthetic composite interfaces and verification of mixing order in cold-recycled asphalt emulsion mixture, *J. Clean. Prod.*, **263** (2020), 121467. https://doi.org/10.1016/j.jclepro.2020.121467
3. J. Zhu, T. Ma, J. Fan, Z. Fang, T. Chen, Y. Zhou, Experimental study of high modulus asphalt mixture containing reclaimed asphalt pavement, *J. Clean. Prod.*, **263** (2020), 121447. https://doi.org/10.1016/j.jclepro.2020.121447
4. Y. Ma, F. Chen, T. Ma, X. Huang, Y. Zhang, Intelligent compaction: An improved quality monitoring and control of asphalt pavement construction technology, *IEEE T. Intell. Transp.*, **23** (2022), 14875–14822. https://doi.org/ 10.1109/TITS.2021.3134699
5. Q. Xu, G. Chang, Evaluation of intelligent compaction for asphalt materials, *Autom. Constr.*, **30** (2013), 104–112. https://doi.org/10.1016/j.autcon.2012.11.015
6. Q. Xu, G. Chang, V. Gallivan, Development of a systematic method for intelligent compaction data analysis and management, *Constr. Build. Mater.*, **37** (2012), 470–480. https://doi.org/ 10.1016/j.conbuildmat.2012.08.001
7. X. Zhao, *Study on Intelligent Compaction Control Technology of Subgrade*, M.S. thesis, Chang'an University in Xi'an, 2016. https://doi.org/10710-2013521093
8. B. Chen, *Research on Real-time Detection System of Subgrade Compaction Degree*, M.S. thesis, Chang'an University in Xi'an, 2019. https://doi.org/10710-2016125023
9. R. Minchin, H. Thomas, Validation of vibration-based onboard asphalt density measuring system, *J. Constr. Eng. M.*, **129** (2003), 1–7. https://doi.org/ 10.1061/(ASCE)0733-9364(2003)129:1(1)
10. H. Zhao, *Study on the Evaluation Index of Roadbed Compaction Quality*, M.S. thesis, Chang'an University in Xi'an, 2015. https://doi.org/10710-2013225045
11. Editorial Department of China Journal of Highway and Transport, Review on China's Pavement Engineering Research·2020, *China J. Highw. Transp.*, **33** (2020), 1–66. https://doi.org/ 10.19721/j.cnki.1001-7372.2020.10.001
12. H. Cui, *Based on Intelligent Compaction Technology of Filling Roadbed Compaction Degree Test Research*, M.S. thesis, Hebei University in Shijiazhuang, 2017. https://doi.org/10075-20151780
13. F. Hao, *Finite Element Analysis of "Vibration Wheel-Soil" Model*, M.S. thesis, Chang'an University in Xi'an, 2007. https://doi.org/10710-20040455

14. Z. Wu, S. Zhang, L. Guo, Application of ABAQUS secondary development in rock breaking simulation of PDC cutter, *J. Xi'an Shiyou Univ.*, **35** (2020), 104–109. https://doi.org/10.3969/j.issn.1673-064X.2020.01.015
15. D. Liu, M. Lin, S. Li, Real-time quality monitoring and control of highway compaction, *Autom. Constr.*, **62** (2016), 114–123. https://doi.org/10.3876 /j.issn.1000-1980.2018.04.005
16. Q. Zhang, T. Liu, Z. Zhang, Z. Huangfu, Q. Li, Z. An, Unmanned rolling compaction system for rockfill materials, *Autom. Constr.*, **100** (2019), 103–117. https://doi.org/10.1016/j.autcon.2019.01.004
17. Z. Wu, S. Zhang, L. Guo, W. Wang, Y. Pan, Application of ABAQUS secondary development in rock breaking simulation of PDC cutter, *J. Xi'an Shiyou Univ.*, **35** (2020), 104–109. https://doi.org/10.3969/j.issn.1673-064X.2020.01.015
18. F. Chen, C. Wang, W. Li, J. Yang, Application of Abaqus secondary development in shot peening strengthening of aerospace arc-shaped frame, *Comp. Aided Eng.*, **29** (2020), 55–60. https://doi.org/10.13340/j.cae.2020.02.011
19. W. Hu, X. Jia, X. Zhu, A. Su, B. Huang, Influence of moisture content on intelligent soil compaction, *Autom. Constr.*, **113** (2020), 103141. https://doi.org/ 10.1016/j.autcon.2020.103141
20. Y. Ma, Y. Luan, W. Zhang, Y. Zhang, Numerical simulation of intelligent compaction for subgrade construction, *J. Cent. South Univ.*, **27** (2020), 2173–2184. https://doi.org/10.1007/s11771-020-4439-2
21. Y. Ma, Z. Fang, T. Han, S. Wang, B. Li, Dynamic simulation and evolution of key control parameters for intelligent compaction of subgrade, *J. Cent. South Univ.*, **52** (2021), 2246–2257. https://doi.org/ 10.11817/j.issn.1672-7207.2021.07.012
22. Y. Ma, Y. Zhang, W. Zhao, X. Ding, Z. Wang, T. Ma, Assessment of intelligent compaction quality evaluation index and uniformity, *J. Transp. Eng. B-Pave.*, **2** (2022), 04022024. https://doi.org/10.1061/JPEODX.0000368
23. X. Teng, *Numerical Analysis and Quality Control of Dynamic Consolidation of Silty Soil Subgrade –in Yellow River Alluvial Plain*, M.S. thesis, Shandong University in Jinan, 2017. https://doi.org/10422-201413217
24. X. Yan, *Some Studies on Functional Linear Regression*, Ph.D. thesis, East China Normal University in Shanghai, 2020. https://doi.org/10269-52164404001
25. Q. Xu, *The Research on Non-Linear Regression Analysis Methods*, M.S. thesis, Hefei University of Technology in Hefei, 2009. https://doi.org/10359-0631111370
26. D. Zhou, *Research on Correlation Optimization of Differential Privacy Regression Analysis Based on Laplace Mechanism*, M.S. thesis, Heilongjiang University in Heilongjiang, 2018. https://doi.org/ 10212 -2151237
27. D. White, P. Vennapusa, H. Gieselman, Field assessment and specification review for roller-integrated compaction monitoring technologies, *Adv. Civ. Eng.*, **2011**, (2011), 1–15. https://doi.org/10.1155/2011/783836

AIMS Press